A Hybrid Polarimetric Wide-Band Beam-former Architecture for 5G mm-Wave Communications

Diego Dupleich[1], Jian Luo[2], Stephan Häfner[1], Robert Müller[1], Christian Schneider[1], and Reiner Thomä[1]
[1]Technische Universität Ilmenau, 98684 Ilmenau, Germany
Email: diego.dupleich@tu-ilmenau.de
[2]Huawei Technologies Düsseldorf GmbH, 80992 München, Germany
Email: jianluo@huawei.com

***Abstract*—Beam-forming at millimeter wave frequencies (mm-wave) is a key technology to fulfill the fifth generation (5G) high data rate requirements. In this paper, we describe a novel hybrid architecture for mm-wave beam-forming, which addresses the mm-wave specific propagation channel characteristics that are identified in recent measurement campaigns. This architecture leverages baseband processing both in analog and digital domain. By enabling multi-beam beam-forming and compensating the polarization mismatch, delay difference (of different beams) and optionally the Doppler shifts (depending on mobility) of the beams at the Tx, a coherent summation of the signals in different beams can be realized, allowing to maximize the signal-to-noise ratio (SNR) and reduce the Rx complexity. Simulations based on measured channels in a typical large indoor scenario have been used to sustain the effectiveness of the proposed beam-forming architecture.**

***Index Terms*—Hybrid beam-forming, multi-beam beam-forming, ultra-wideband communications, polarization, mm-Wave, 5G**

I. Introduction

5G mobile and wireless communication systems are expected to support the explosive growth of wireless traffic in the order of 1000 times from 2010 to beyond 2020 [1]. Considering the spectrum shortage situation in the sub-6 GHz bands [2] and the limited space for spectral efficiency enhancement, such wireless traffic growth can only be realized when the large amount of bandwidth in the mm-wave frequency bands is exploited. The exploitation of the mm-wave frequencies faces several challenges [3]. One of the most typical challenges is that the free space path loss (with isotropic radiation) increases with the square of the frequency and becomes significantly higher than that of sub-6 GHz frequencies. A further important challenge is the penetration loss and the resulting vulnerability to blockage. Fortunately, with increased frequency, the size of the antenna elements decreases, such that the number of antenna elements that can be packed into a given area can also increase with the square of the frequency. Thus, for a given physical antenna aperture, communication at mm-wave is able to benefit from a larger antenna gain which can compensate the adverse effect of high path loss. Accordingly, beam-forming with large antenna arrays at both transmitter (Tx) and receiver (Rx) is expected to be a key technology for mobile radio communication at mm-wave frequencies.

Due to the large dimensionality of the Tx/Rx antenna arrays and the large bandwidths envisioned for mm-wave communication, a full digital implementation of the multiple-input / multiple-output (MIMO) transceivers becomes very challenging. The reason is that a large amount of RF chains and high resolution high speed converters (DAC/ADC) are needed, which increase the hardware complexity and power consumption significantly increases as well. A possible approach to address this challenge is the so called "hybrid beam-forming (HBF)" [4], where part of the beam-forming operations are performed in the analog domain and the other part in the digital baseband. In this way, the number of required RF chains and/or converters can be significantly reduced. Compared to pure analog beam-forming (with only one RF chain and one DAC/ADC), hybrid beam-forming has the advantage of supporting multiple streams and more flexibility. Although full digital beam-forming delivers the maximum performance, hybrid beam-forming is able to provide a trade-off between performance and implementation complexity as well as power consumption.

In this paper, we propose a hybrid beam-forming architecture that applies baseband analog processing and is designed properly according to the specific characteristics of the mm-wave propagation channel. From measurements, it can be seen that the mm-wave channel presents a sparse characteristic in the directional / delay domain with strong reflected paths showing deterministic characteristics, [5]–[7]. Accordingly, high gain sharp pencil beams that can be oriented to match the strongest paths can be generated with large antenna arrays. Multiple beams can be used to increase received power, link robustness e.g. to overcome shadow fading and to increase the capacity. Depending on the channel condition and link budget, different beam-forming strategies can be applied. For MIMO channel with rich scattering, spatial multiplexing (SM) [8] can significantly increase capacity in high SNR regimes. For the sparse mm-wave channels in low SNR regimes, beam-forming (BF) is more desired to increase the SNR. In fact, both SM and BF can be combined, e.g. if there are degrees of freedom available after performing BF to achieve a target SNR, such degrees of freedom can be used for spatial multiplexing to further increase the capacity.

In most of the MIMO studies, total power constraint or

per antenna power constraint are assumed. However, for mm-wave communication, the regulation may also restrict the equivalent isotropically radiated power (EIRP), implying that when applying beam-forming, the Tx power per beam is restricted. In this case, the coherent combination of multiple beams at the receiver might allow to reach the link budget without violating such regulation. The performance of mm-wave multi-beam-forming has been analysed in [8], [9].

It has also been observed that in mm-wave channels, polarization plays an important role, especially in power limited regimes. As shown in [10], a mismatch in the Tx-Rx antenna polarization alignment results in a drastic reduction in the link budget. To overcome this problem, polarimetric filters can be applied in combination with beam-forming. The application of polarimetric filters has been discussed in [11], [12].

Based on the above listed special characteristics of the mm-wave propagation channels, we introduce a transceiver architecture in this paper, which is a hybrid beam-forming architecture allowing multi-beam beam-forming with polarization matching as well as delay difference (of different beams) and Doppler compensation. The proposed beam-forming architecture and the corresponding scheme can maximize the received signal quality by exploiting the signal energy in different propagation paths. The beam-former consists of multiple digital interfaces (DAC/ADC) with individual analog beam-forming structures with the capability to compensate for polarization mismatch, delay difference, and Doppler. Each data stream is precoded and transmitted over multiple pencil beams. By compensating the polarization mismatch, delay difference, and optionally the Doppler shifts (depending on mobility) of the beams at the Tx, a coherent summation of the signals in different beams can be realized, allowing to maximize the SNR and reduce the Rx complexity. By compensating the delay difference of different beams, inter-symbol interference (ISI) can be significantly reduce or even eliminated.

The paper is organized as follows: in Section II we describe a measurement campaign in a typical 5G large indoor scenario and the identified mm-wave specific propagation characteristics that guides the design of the proposed architecture. In Section III we introduce the architecture of the analog polarimetric multi-beam beam-former with the capabilities to address the propagation characteristics at mm-wave. Section IV shows performance figures of such a beam-former using the measurement data and verifies the benefit of the proposed architecture. Finally, Section V summarizes the findings in this paper.

II. Propagation Characteristics from Measurements at mm-Wave

A. Scenario and Measurement Description

To derive the mm-wave specific propagation charateristics, several measurement campaigns have been carried out [5]–[7]. Here, we observe one of the most typical one in a large indoor scenario in the 70 GHz band. In this measurement campaign, double-directional dual-polarized ultra-wideband measurements were carried out in a large entrance hall at the Technische Universität Ilmenau (TU Ilmenau). These measurements are an extension of the ones introduced in [7]. Figure 1 shows the transceiver locations, where different Tx and Rx positions were measured. The Tx - Rx link combinations and visibility conditions are addressed in Table I. The difference of height between the Tx and Rx locations, the quantized measured angles, and the fact that elevation was not scanned at the Rx introduces a misalignment of the Tx and Rx antenna pointing directions in the line of sight (LOS). Since we don't have pure LOS measurements, we denominate it non-aligned line of sight (NaLOS).

The dual-polarized ultra wide-band multi-channel sounder (DP-UMCS) used in this campaign is introduced in [14]. The $3\,\mathrm{dB}$ bandwidth after calibration is $4\,\mathrm{GHz}$ [7]. Double-directional measurements were carried out using high directive horn antennas with 15° half-power beam-width (HPBW) both at the Tx and Rx side. The measured antenna patterns can be seen in Figure 2. The Tx was located in three different floors always higher than the Rx representing the location of a typical access point. The Rx were located always in the ground floor at a lower height as the handsets of the users. A 3D positioner with an azimuth over elevation (Az/El) coordinate system was used at the Tx, measuring azimuth in 15° steps $\phi_{\mathrm{Tx}} \in [-90^\circ, 90^\circ]$ and elevation $\theta_{\mathrm{Tx}} \in [-45^\circ, 45^\circ]$. In contrast, only azimuth $\phi_{\mathrm{Rx}} \in [-180^\circ, 165^\circ]$ was measured at the Rx.

It is important to notice that the non-line of sight (NLOS) condition in the links Tx1 with Rx9 and Rx10 is different to Tx2 and Tx3 with Rx2, Rx3, and Rx4, since the NLOS condition in the first case results from the obstruction by structures (stairway and cabinets) and the NaLOS in the second case is due to a mismatch of the directivity of the antennas and the scanned elevation range.

B. Post-processing of the Measurements

The noise floor is estimated and removed from the measurements to avoid considering noise as channel samples. The estimation is performed by analysing the cumulative distribution of each measured channel impulse response (CIR), following a similar procedure as [15]. All the samples lower than the noise floor plus a margin of $10\,\mathrm{dB}$ were set to zero.

Furthermore, since the 3D positioner system tilts the antenna in a different angle for each azimuth and elevation position, a correction of the polarization coordinate system was performed synthetically to keep the Tx horizontal polarization parallel to the floor plane, and the vertical perpendicular to it, as described in [6].

Since in this paper we focus on an analysis of system performance (instead of the channel itself), the bandwidth was reduced to $500\,\mathrm{MHz}$ to target a system with an application bandwidth closer to the ones discussed on recent publications as [8]. The reduction was performed by applying a root raised cosine filter with a roll-off factor $\beta = 0.35$ and decimating the measured CIR to reach a sampling rate of $500\,\mathrm{MHz}$.

Table I
TX - RX VISIBILITY DESCRIPTION IN THE LARGE HALL SCENARIO.

	RX1	RX2	RX3	RX4	RX5	RX6	RX7	RX8	RX9	RX10
TX1	NaLOS	NaLOS	NaLOS	NaLOS	NaLOS	NaLOS	NaLOS	NaLOS	NLOS	NLOS
TX2	NaLOS	NLOS	NLOS	NLOS	-	-	-	-	-	-
TX3	NLOS	NLOS	NLOS	NLOS	NLOS	NLOS	NLOS	NLOS	-	-

C. Spatio - Temporal Characteristics of the Propagation Paths

Figure 3 shows the spatio - temporal characteristic of the channel after selecting the two strongest beams at the Tx by means of the power azimuth / delay profile (PADP) at the Rx for the NaLOS link Tx1 - Rx7 and NLOS link Tx1 - Rx10. Paths are arriving from different directions at different time instances. In the first case, the NaLOS component is dominant and the other beams are negligible in comparison to the strongest one. In this case, using multiple beams is not efficient since the remaining beams don't provide sufficient energy to the link budget. However, they can be used as back up link in case the NaLOS component is blocked. In the second case (Figure 3b), the energy is distributed more equivalently between the different beams and increases the received power.

The number of channel taps (and excess delay window) is also reduced if a lower dynamic range is applied. In the present work we consider a dynamic range of $20\,\mathrm{dB}$. However, some other authors consider multipath within a range of only $10\,\mathrm{dB}$ [8].

The high resolution in the time domain provided by the large bandwidth and in the directional domain provided by the high order antenna arrays, results in a distribution of the channel taps as shown in Figure 3. These paths tend to be clear in terms of fading, due to the low superposition they experience.

Based on the measured data, three different cases of spatial temporal distribution of CIR can be summarized, as shown in Figure 4, in which the columns are the Tx - Rx beams, and the rows are the delay taps of the channel.

Case I is the ideal one where each beam has a single delay tap and for instance the implementation of a spatio-temporal beam-former is simplified since each beam observes a narrowband channel that requires no equalization; case II has several channel taps per beam, in which equalization per beam has to be implemented; and case III has several beams per delay tap. In the latest case, multiple beams can be formed simultaneously to address those components that arrive at the same time, or zeros can be steered in the directions of undesired components.

The equalization requirements are associated to the delay spread (DS). However, also DS depends on the relation between beam-width and size of scatterers. High-directive beams tend to reduce the DS by addressing single scatterers. It can be observed that the intra-beam DS is reduced in comparison to omni-directional cases [7]. However, the total DS considering several beams is considerably large compared to per beam DS. For example, in Figure 3b, there are approx. 36 channel taps considering all the beams, but 3 delay taps for Tx beam #1, and approx. 9 for Tx beam #2. For instance, to save resources, equalization has to be performed individually per-beam, and not as the composition of several beams.

D. Polarimetric Characteristics

The polarization changes with the interaction of the waves with the environment. In particular, due to the small size of the wavelength, the number of objects that affect the propagation path by interacting and changing the polarization properties is increased. These changes can be the rotation of the linear polarization angle, or the cancellation of a determined polarization after the interaction with structures that only reflects one of the components of the polarization.

Figure 5 shows the power normalized PADP for the Tx1 - Rx10 link (Figure 3b decomposed in the polarimetric components). It can be observed that the different paths have a different polarimetric scattering footprint. Tx beam 1 shows no preference to either V or H polarization. On the other hand, Tx beam 2 has a predominant V polarization characteristic. This is the result of a scattering process (or multiple processes) that suppress the H polarization.

Previous measurements in an in-door scenario at mm-waves showed that the polarization state of the main paths tend to be clear [6]. This is a consequence of clear paths. In order to maximize the received power, the polarization has to be individually optimized per beam by means of polarimetric filters. A polarimetric filter combines coherently the signal of orthogonal polarizations to synthesize a certain polarization of the radiated signal in order to either maximize the received power, or to minimize it. For example, undesired paths can be suppressed to reduce DS or interference from other users [11].

E. Doppler Characteristics

Doppler information couldn't be extracted from these measurements since only static scenarios were measured. However, we assume that each beam might experience a different Doppler effect due to the relative position and movement of the scatterers, specially, in high dynamic scenarios as trains, vehicular-to-vehicular (V2V), etc.

If the beams carry a relatively small DS as shown in the previous subsections, the channel can be considered consisting of single or few number of taps and for instance, the Doppler effect would rather be a shift than a spread. This can be mitigated by a per-beam Doppler shift compensation on the carrier frequency. As a direct consequence, the coherence time would also be increased.

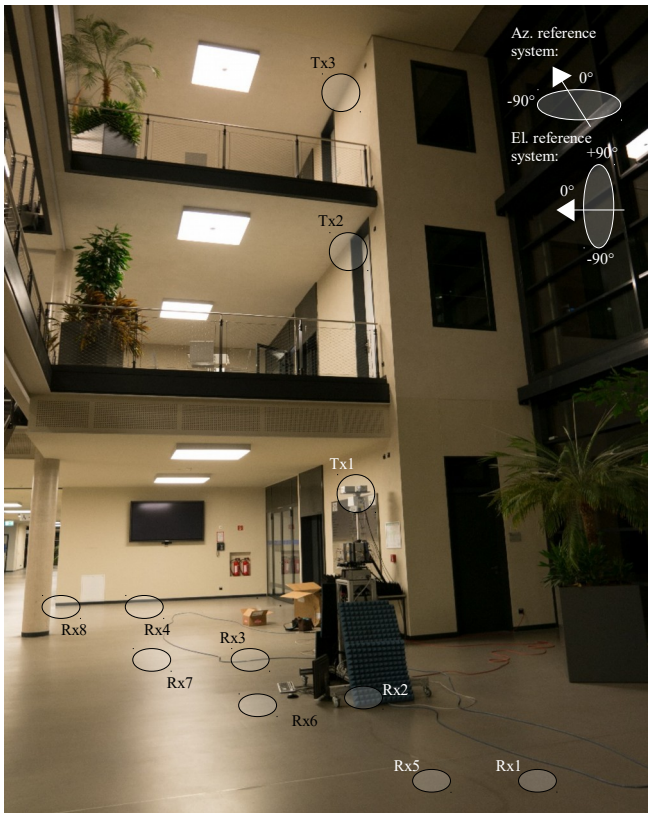

(a) Front view of the entrance hall. Position of the TX1, TX2, and TX3.

(b) View of the remaining RX positions in the entrance hall.

Figure 1. Entrance hall scenario.

F. Spatial Characteristics for Multiple Access

In the case of multiple users, BF can be used to provide access to different users by steering beams in the direction of different users and/or scatterers. However, under NLOS conditions and when using multiple beams for a single user, the scarce number of scatterers might result in users sharing Tx beams, as shown in Figure 6. This analysis considers the three strongest beams at Tx1 for all the Rx positions (ten in total), considering BF at Tx and an omni-directional Rx. The

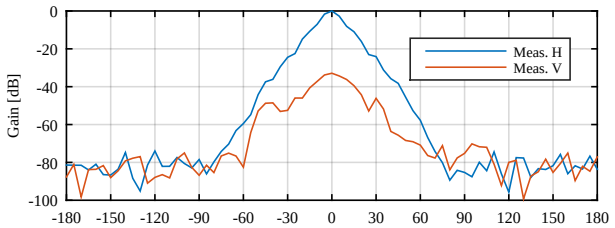

(a)

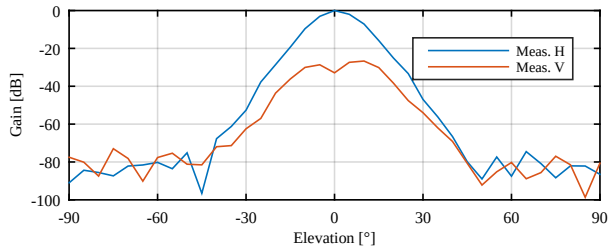

(b)

Figure 2. Measured antenna pattern used during the measurements.

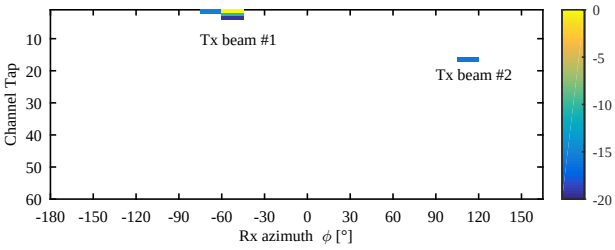

(a)

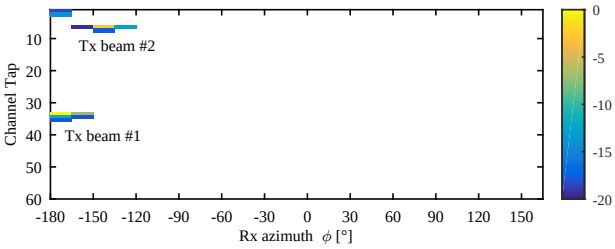

(b)

Figure 3. PADP at the Rx for the strongest beams at Tx: (a) NaLOS link Tx1 - Rx7 and (b) NLOS link Tx1 - Rx10.

histogram shows that several beams are shared by all users (beams that have an occurrence higher than one).

The polarization dimension can also be used to provide access to different users that share the same Tx beams. However, a deeper analysis has to be done on the rank of the polarimetric scattering matrix per beam, in order to quantize the available polarization diversity.

III. Hybrid Polarimetric Beam-Former Architecture

The aim of this architecture is to address the spatio - temporal matrix (i.e., via multi-beam and delay difference compensation), polarization, and Doppler characteristics introduced in

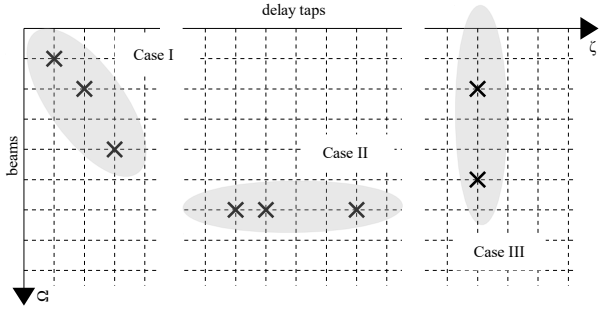

Figure 4. Different cases of the spatio - temporal matrix.

Section IV-B. This architecture is a hybrid architecture consisting of analog- and digital baseband processing. Specifically, in the analog baseband processing, Gilbert cells can be used to implement real or complex valued multiplications, e.g., for the weighting operations of the beam-forming or the polarimetric filtering. In this way, the analog domain beam-former has similar capabilities of a digital beam-former, except for the frequency selective (subcarrier dependent) beam-forming. Note that in this paper, we mainly focus on the structure of the transceiver architecture. For the optimization and computation of the BF coefficients, please refer to our recent paper [12].

Figure 7 shows the case of a system that benefits the cellular downlink transmission with most of the processing at Tx side and a simple Rx architecture with dual-polarized low directional characteristics. For simplicity, we mainly describe the architecture for the case of single user and single data stream. However, extension to multi-data stream using SM is possible. When there are multiple of the BF circuits (described below) with multiple digital interfaces at Tx and/or Rx, MIMO or multi-user MIMO (MU-MIMO) can be performed on top of the effective channel matrices after the analog BF.

The Tx has $M_\mathrm{T}/2$ dual-polarized antennas, and for instance M_T beam-former coefficients per BF structure. Each BF structure $\mathbf{w}_{\mathrm{T},i}(\alpha_{\mathrm{T},i}, \mathbf{\Omega}_{\mathrm{T},i}) \in \mathbb{C}^{M_\mathrm{R}\times 1}$ is in charge of steering the beams in the $\mathbf{\Omega}_{\mathrm{T},i}$ direction of departure (DoD) and match the α_i linear polarization (where α is the linear polarization angle). Elliptical polarization can also be synthesized by adding a phase difference between the coefficients of $\mathbf{w}_{\mathrm{T},i}$ for the H and V antennas. Compared to digital BF, the number of digital interfaces for data signal is reduced from M_T to N_T. Each digital interface can address a different user in a multi-user scenario, different data streams N_s for a single user, or different delayed beams also for a single user. $M_R/2$ is the number of dual-polarized antennas at the Rx. If we consider a single dual-polarized antenna as shown in Figure 7, $\mathbf{w}_{\mathrm{R},j}(\alpha_{\mathrm{R},j})$ is only in charge of optimizing the polarization of the impinging signals. On the other hand, if we consider an array at the Rx, $\mathbf{w}_{\mathrm{R},j}(\alpha_{\mathrm{R},j}, \mathbf{\Omega}_{\mathrm{R},j})$ is in charge of steering the beams in the $\mathbf{\Omega}_{\mathrm{R},j}$ direction of arrival (DoA) and optimizing individually the polarizarion α_R per beam for a coherent summation (Figure 8a). If SM is applied, $N_s > 1 \rightarrow N_\mathrm{R} = N_s$ and each $\mathbf{w}_{\mathrm{R},j}$ is connected to a different digital interface, as shown in Figure 8b. The system equation can be written as:

$$\mathbf{y}(t) = \mathbf{\Sigma}\mathbf{W}_\mathrm{R}^H \sum_\tau \mathbf{H}(t-\tau)\mathbf{W}_\mathrm{T}\mathbf{x}(t) + \mathbf{\Sigma}\mathbf{W}_\mathrm{R}\mathbf{n}(t), \qquad (1)$$

where $\mathbf{x}(t) \in \mathbb{C}^{N_s\times N_\mathrm{T}}$ is the pre-coded signal, and $\mathbf{y}(t) \in \mathbf{C}^{N_\mathrm{R}\times N_s}$ is the received signal, $\mathbf{H}(\tau) \in \mathbb{C}^{M_\mathrm{R}\times M_\mathrm{T}}$ is the channel matrix, $\mathbf{W}_\mathrm{R} \in \mathbb{C}^{M_\mathrm{R}\times N_\mathrm{R}}$ is the beam-former at the Rx, and $\mathbf{W}_\mathrm{T} \in \mathbb{C}^{M_\mathrm{T}\times N_\mathrm{T}}$ is the beam-former at the Tx. The columns of $\mathbf{W}_\mathrm{R}$ and $\mathbf{W}_\mathrm{T}$ ar the previously defined beam-former vectors $\mathbf{w}_\mathrm{R}$ and $\mathbf{w}_\mathrm{T}$, respectively. $\mathbf{\Sigma} \in \mathbb{R}^{N_\mathrm{R}\times N_s}$ depends on the implementation. If we consider a single data stream, then $\mathbf{\Sigma} = [1, \cdots, 1]\,\mathbb{R}^{1\times N_\mathrm{R}}$. On the other hand, if we consider SM, then $\mathbf{\Sigma} = \mathbf{I}_{N_\mathrm{R}\times N_\mathrm{R}}$.

The channel in the digital domain is represented as the beam-space channel matrix $\mathbf{H}_\mathrm{BS}(\tau) \in \mathbb{C}^{N_\mathrm{R}\times N_\mathrm{T}}$. This is the effective digital channel after analog BF, where τ is the delay index:

$$\mathbf{H}_\mathrm{BS}(\tau) = \mathbf{W}_\mathrm{R} \sum_\tau \mathbf{H}_\mathrm{BS}(t-\tau)\mathbf{W}_\mathrm{T}. \qquad (2)$$

We assume a Tx with a high order antenna array capable of generating narrow beams with a high spatial resolution. On the other hand, the Rx can have antennas with broader beams due to a smaller number of antennas and less computation capabilities. Furthermore, the large bandwidth of the signals allows a high temporal resolution, so that the multi-path components of the channel can be identified in the delay domain. Moreover, according to the measurement results, the polarization of the channel taps are quite clear [6]. The reason is that the paths are more deterministic and not the result of a sum of multiple paths close to each other in the delay domain.

The beam-former at Tx is in charge of selecting the stronger paths, adjusting the polarization to enhance or suppress desired or undesired paths, compensating Doppler shift, and equalizing and aligning the delay of each beam. For simplicity, the Rx is considered omni directional or have broad fixed beam with dual-polarized antennas.

A detailed scheme of the beam-former implementation for down-link is shown in Figure 9. A similar architecture can be implemented also for up-link, where the BF processing is mainly done at the Rx. The beam-former coefficients are calculated in the digital domain, but applied to the data signal in the analog domain with multiplications implemented using Gilbert cells. The complex multiplications are unfolded in real multiplications.

The beam-former first selects in the spatial domain the beams that correspond to the strongest propagation paths. After the selection of the main beams, the polarization is optimized to either increase the signal power at the receiver or to suppress it if is causing interference to other users. The polarization can be either linear or elliptical. It depends only on the phase difference between the BF coefficients of the orthogonally polarized antennas.

If there are multiple channel taps within a single beam, there will be inter-symbol interference (ISI) inside the beam, which can not be compensated by the delay difference compensation.

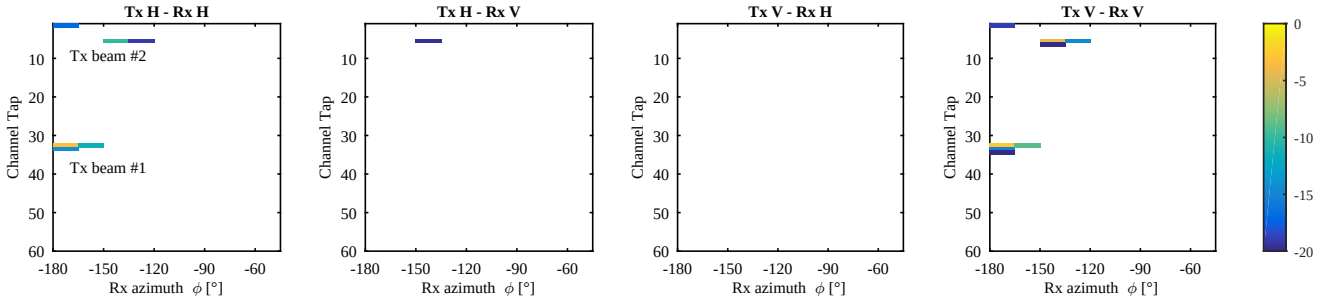

Figure 5. Polarimetric decomposition of the PADP at Rx considering the two strongest beams for the link Tx1 - Rx10.

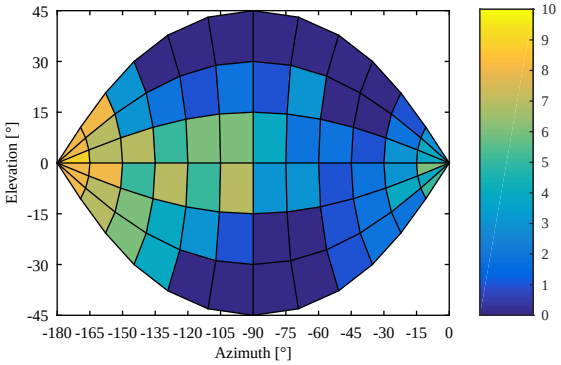

Figure 6. Histogram showing the number of beams distributed in the azimuth and elevation at the Tx1.

Such ISI can be further compensated either by the pre-coder at Tx and the equalizer at Rx.

Note that in other literatures, e.g., [4], radio frequency (RF) phase shifters are assumed to be used for the beam-forming operation. Our approach of polarimetric filter, delay difference, and Doppler compensation can also be applied to such RF phase shifter based beam-formers, e.g., by introducing additional analog baseband or RF processing.

Finally, it should be remarked that due to delay compensation in the pre-coder, the frequency selectivity of the channel can be mitigated. Frequency selective (subcarrier dependent) BF (as in sub-6 GHz MIMO) that requires full digital beam-forming architecture becomes unnecessary. This further motivates the analog implementation of the BF processing, which can not be frequency selective but has the advantages of reduced hardware complexity and power consumption.

IV. Results

In this section, we show the performance of multi-beam beam-forming (with delay difference compensation implicitly included) and the polarimetric optimization by using the measured channel data of the scenario described in Section II. Due to missing measurement data in mobility scenarios, the performance of Doppler compensation cannot be shown here and remains future work.

A. Multi-beam Beam-forming Gain

The use of multiple beams can be used to either increase robustness against shadowing and/or increase the signal power at the receiver to meet a SNR criteria, specially under power limited conditions. Note that in our evaluation here, the delay difference compensation is implicitly included.

Figure 10 shows the received power gain compared to the strongest beam, if multiple beams are used at the Tx and with an omni-directional Rx, based on the measurements for NaLOS and NLOS conditions. It is worth to mention that the beam-steering process was emulated by the rotation of the antennas during the measurements. As a consequence, the performance correspond to a beam-former with fixed beams. A real implementation of the architecture introduced in this paper would consider adaptive beams. On the other hand, analog adaptive steerable antennas in practice introduce some additional losses due the adaptivity, which might reduce the obtained gains. In this paper, equal gain combining (EGC) was used as criteria. As expected, it can be seen that in the NaLOS case there is not a big difference between adding 2 or 3 beams due to the strong NaLOS component. However, in the NLOS scenario the difference is bigger, and also the gain compared to a single beam is larger. On average, 3 dB can be gained by using 3 beams in NLOS conditions.

B. Polarimetric Optimization

Figure 11 shows the cumulative distribution function (CDF) of the gain obtained after applying polarimetric optimization individually to the three main beams of all the measured links. The polarimetric filter is selected as a matched filter to the strongest delay tap at Rx, receive polarization optimization (RPO); at the Tx, transmit polarization optimization (TPO); and jointly at Tx and Rx by applying singular value decomposition (SVD) to the polarimetric matrix of the strongest delay tap, joint polarization optimization (JPO). The gain is calculated in comparison to the maximum received power per beam considering single polarization (polarization selection). A different polarization optimization criteria could also be applied using this architecture. It can be observed that in most of the cases JPO offers the highest gain compared to polarization selection (selecting the combination of polarization that delivers more energy without any processing). However, there are cases with 0 dB gain. This are the cases where for

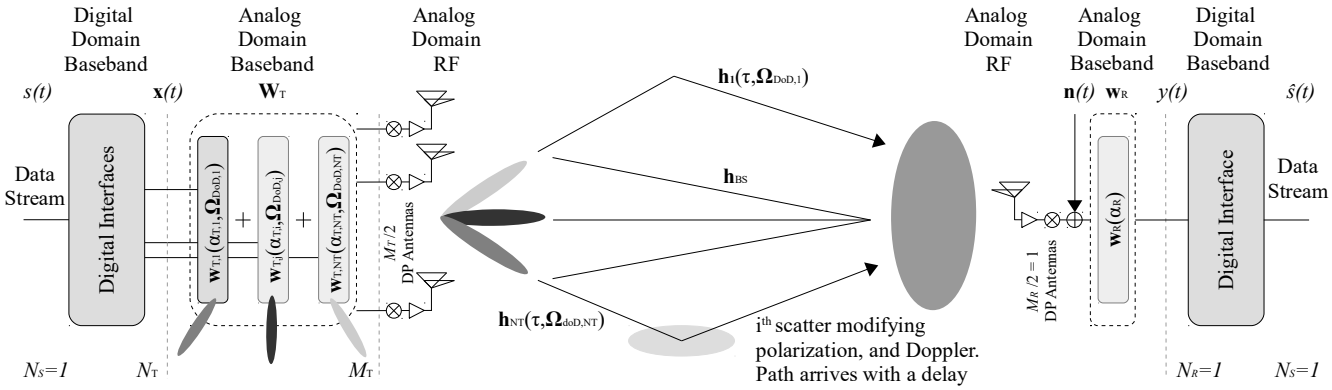

Figure 7. System architecture and schematic of the beam-former.

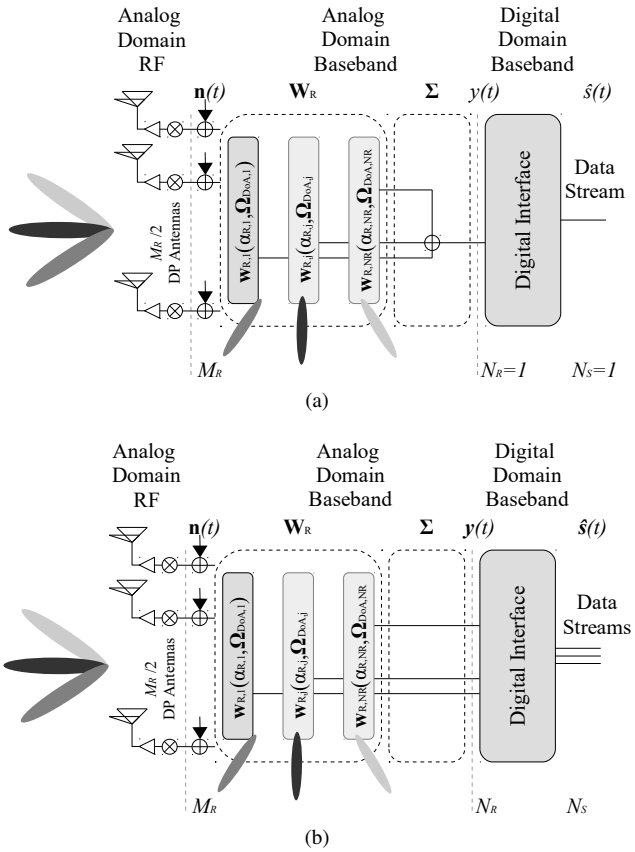

Figure 8. Alternative Rx implementation considering (a) single data-stream multi-beam BF, and (b) SM.

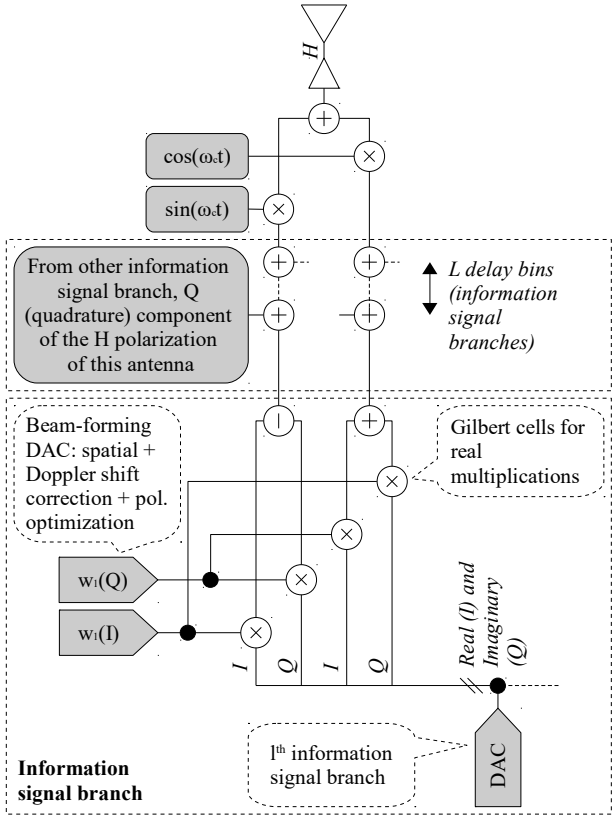

Figure 9. Implementation of the polarimetric analog beam-former using Gilbert cells.

example there is energy in only one of the polarizations, or there are multiple paths carrying different polarizations that are not optimized with a single polarimetric filter.

V. Conclusions

In this paper we have introduced a hybrid polarimetric wide-band beam-forming architecture that addresses the mm-wave propagation characteristics derived from recent measurements.

The sparse spatio-temporal characteristic of the channel, due to the high directive antennas and bandwidth, allows the identification of paths with different angle of arrivals and times of arrivals. Treating these paths individually simplifies the implementation of equalization and focusing the energy on the scatterers improves the energy efficiency.

Due to delay compensation in the pre-coder, the frequency selectivity of the channel can be mitigated. On the one hand, the Rx signal power can be enhanced and frequency selective beam-forming that requires full digital beam-forming architecture becomes unnecessary. This facilitates the analog implementation of the BF processing.

The use of multiple beams per user to increase the received

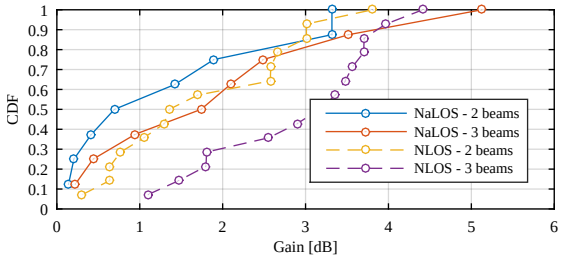

Figure 10. Gain compared to the main beam after adding 2 and 3 beams, considering Tx BF and omni-directional Rx.

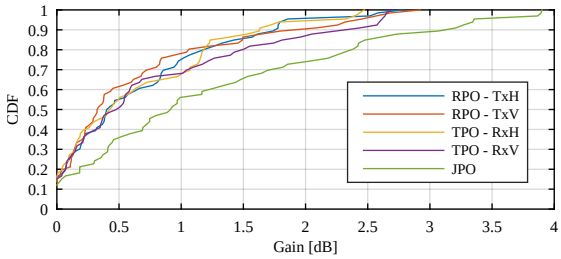

Figure 11. Gain of the polarimetric optimization per beam at different sides.

signal power has been analysed and shows a considerable enhancement of the Rx signal power. This is more noticeable under NLOS conditions, where the difference between the power of different beams is small, and/or under EIRP constraints.

A mismatch between the Tx and Rx polarization due to change on the polarization characteristics after reflections or movement of antennas reduces the received energy. Optimizing the polarization by electronically adjusting the signal ratios and phase of the beams to meet the polarimetric characteristics of the scatters and/or received antennas showed an improvement of the received energy. This optimization can be performed at Tx, Rx, or jointly, showing the latest a higher gain.

The compensation of Doppler shifts of different beams has also been proposed in this architecture. The evaluation of the corresponding performance remains for future work.

REFERENCES

[1] A. Osseiran, V. Braun, T. Hidekazu, P. Marsch, H. Schotten, H. Tullberg, M. A. Uusitalo, and M. Schellman, "The Foundation of the Mobile and Wireless Communications System for 2020 and Beyond: Challenges, Enablers and Technology Solutions," in *2013 IEEE 77th Vehicular Technology Conference (VTC Spring)*, pp. 1–5.

[2] J. Luo, J. Eichinger, Z. Zhao, and E. Schulz, "Multi-carrier waveform based flexible inter-operator spectrum sharing for 5g systems," in *Dynamic Spectrum Access Networks (DYSPAN), 2014 IEEE International Symposium on*, April 2014, pp. 449–457.

[3] M. Nekovee, P. V. Wrycza, M. Fresia, M. Peter, J. Gora, J. Luo, and M. Tesanovic, "Millimetre-wave based mobile radio access network for fifth generation integrated communications (mmMAGIC)," *European Conference on Networks and Communications (EuCNC'15)*, Juluy 2015.

[4] A. Alkhateeb, Jianhua Mo, N. Gonzalez-Prelcic, and R. W. Heath, "MIMO Precoding and Combining Solutions for Millimeter-Wave Systems," *IEEE Communications Magazine*, vol. 52, no. 12, pp. 122–131, 2014.

[5] D. Dupleich, F. Fuschini, R. Mueller, E. Vitucci, C. Schneider, V. Degli Esposti, and R. S. Thomae, "Directional characterization of the 60 GHz indoor-office channel," in *2014 XXXIth URSI General Assembly and Scientific Symposium (URSI GASS)*, pp. 1–4.

[6] D. Dupleich, S. Haefner, C. Schneider, R. Mueller, R. S. Thoma, J. Luo, E. Schulz, X. Lu, and G. Wang, "Double-Directional and Dual-Polarimetric Indoor Measurements at 70 GHz," *2015 IEEE 26th International Symposium on Personal Indoor and Mobile Radio Communications (PIMRC)*, 2015.

[7] S. Haefner, D. Dupleich, R. Mueller, C. Schneider, R. S. Thomae, J. Luo, E. Schulz, X. Lu, and T. Wang, "Characterisation of Channel Measurements at 70GHz in Indoor Femtocells," *2015 IEEE 81st Vehicular Technology Conference*, 2015.

[8] S. Sun, T. S. Rappaport, R. W. Heath, A. Nix, and S. Rangan, "MIMO for Millimeter-Wave Wireless Communications: Beamforming, Spatial Multiplexing, or Both?" *IEEE Communications Magazine*, 2014.

[9] V. Degli-Esposti, F. Fuschini, E. M. Vitucci, M. Barbiroli, M. Zoli, L. Tian, X. Yin, D. A. Dupleich, R. Mueller, C. Schneider, and R. S. Thomae, "Ray-Tracing-Based mm-Wave Beamforming Assessment," *IEEE Access*, vol. 2, pp. 1314–1325, 2014.

[10] A. Maltsev, E. Perahia, R. Maslennikov, A. Sevastyanov, A. Lomayev, and A. Khoryaev, "Impact of Polarization Characteristics on 60-GHz Indoor Radio Communication Systems," *IEEE Antennas and Wireless Propagation Letters*, vol. 9, pp. 413–416, 2010.

[11] D. E. Berraki, S. M. D. Armour, and A. R. Nix, "Polarimetric filtering for an enhanced multi-user 60GHz WPAN system," in *2014 IEEE Wireless Communications and Networking Conference (WCNC)*, pp. 347–351.

[12] D. Dupleich, S. Haefner, C. Schneider, R. Mueller, R. S. Thomae, J. Luo, E. Schulz, X. Lu, and G. Wang, "Real-field Performance of Multiple-beam Beam-former with Polarization Compensation," *10th European Conference on Antennas and Propagation (EuCAP)*, 2016.

[13] R. Muller, S. Hafner, D. Dupleich, J. Luo, E. Schulz, R. Herrmann, C. Schneider, R. S. Thoma, X. Lu, and T. Wang, "Ultra-wideband channel sounder for measurements at 70 ghz," in *Vehicular Technology Conference (VTC Spring), 2015 IEEE 81st*, May 2015, pp. 1–5.

[14] R. Mueller, R. Herrmann, D. A. Dupleich, C. Schneider, and R. S. Thomae, "Ultrawideband multichannel sounding for mm-wave," in *2014 8th European Conference on Antennas and Propagation (EuCAP)*, pp. 817–821.

[15] A. Bottcher, C. Schneider, P. Vary, and R. S. Thomae, "Dependency of the power and delay domain parameters on antenna height and distance in urban macro cell," in *Antennas and Propagation (EUCAP), Proceedings of the 5th European Conference on*, 2011, pp. 1395–1399.